C. R. Mecanique 338 (2010) 434–449

Contents lists available at ScienceDirect

Comptes Rendus Mecanique

www.sciencedirect.com

Inverse problems

Nodal predictive error model and Bayesian approach for thermal diffusivity and heat source mapping

Modèle nodal basé sur l'erreur de prédiction et approche bayésienne pour la cartographie de diffusivité thermique et de terme source

H. Massard [a,b,c], Olivier Fudym [b,c,d,*], H.R.B. Orlande [a], J.C. Batsale [d]

[a] *PEM/COPPE, Federal University of Rio de Janeiro, Brazil*
[b] *Université de Toulouse, mines Albi, CNRS, campus Jarlard, 81013 Albi cedex 09, France*
[c] *École des mines Albi, centre RAPSODEE, campus Jarlard, 81013 Albi, France*
[d] *TREFLE-ENSAM, UMR 8508 CNRS, 33405 Talence cedex, France*

ARTICLE INFO

Article history:
Available online 16 August 2010

Keywords:
Heat transfer
Thermal diffusivity mapping
Heat source mapping
Infrared image processing
Metropolis–Hastings
Inverse problem
Bayesian estimation

Mots-clés :
Transferts thermiques
Champ de diffusivité thermique
Cartographie de terme source
Traitement d'images infrarouges
Metropolis–Hastings
Problèmes inverses
Estimation bayésienne

ABSTRACT

This article aims at solving a two-dimensional inverse heat conduction problem in order to retrieve both the thermal diffusivity and heat source field in a thin plate. A spatial random heat pulse is applied to the plate and the thermal response is analysed. The inverse approach is based on the minimisation of a nodal predictive error model, which yields a linear estimation problem. As a result of this approach, the sensitivity matrix is directly filled with experimental data, and thus is partially noisy. Bayesian estimators, such as the Maximum A Posteriori and a Markov Chain Monte Carlo approach (Metropolis–Hastings), are implemented and compared with the Ordinary Least Squares solution. Simulated temperature measurements are used in the inverse analysis. The nodal strategy relies on the availability of temperature measurements with fine spatial resolution and high frequency, typical of nowadays infrared cameras. The effects of both the measurement errors and of the model errors on the inverse problem solution are also analysed.

RÉSUMÉ

Un problème de conduction 2D est traité pour estimer un champ de diffusivité thermique et terme source sur une plaque mince. Un flash photothermique spatiallement aléatoire est appliqué à la plaque et on analyse le champ de réponse thermique. L'inversion est abordée en minimisant un modèle basé sur l'erreur de prédiction, ce qui permet de rester dans un cadre d'estimation linéaire. Une conséquence directe est que la matrice de sensibilité est construite avec les données expérimentales, et donc contient des erreurs de mesures. On développe des estimateurs bayésiens tels que l'estimateur du Maximum à Postériori ou dans le cadre des algorithmes de Monte Carlo et Chaînes de Markov (Metropolis–Hastings), pour les comparer à la solution des Moindres Carrés Ordinaires. Les résultats sont obtenus à partir de données simulées. L'approche nodale est liée à l'obtention de mesures par thermographie infrarouge. On analyse à la fois l'effet des erreurs de mesures et des erreurs de modèles sur les résultats de l'estimation.

* Corresponding author at: École des mines Albi, centre RAPSODEE, campus Jarlard, 81013 Albi, France.
E-mail address: fudym@mines-albi.fr (O. Fudym).

1631-0721/$ – see front matter
doi:10.1016/j.crme.2010.07.015

1. Introduction

The mapping of thermophysical properties from thermal images provided by an infrared camera is a difficult inverse problem, due to both the large amount of measured data to be processed and the elevated number of parameters to be estimated, as well as the low signal-to-noise ratio. It is thus of interest to implement a linear estimation approach, in order to obtain low computational costs, which can be achieved by minimising a prediction error model instead of an output error model [1]. Usual inversion methods implemented so far to retrieve the parameter fields are generally based on local estimation algorithms that study correlations between pixels. Moreover, in the case of the heat pulse response analysis, the signal-to-noise ratio can be increased by applying a spatially random heat pulse heating [2]. Unfortunately, this kind of approach makes it necessary to fill in the sensitivity matrix directly with some linear operations on the measured data. Then the stochastic nature of the regression matrix may yield a bias in the estimates when an ordinary least squares approach is computed. In a previous work, this problem was addressed with the Total Least Squares (TLS) estimation method [3].

In this article, we make use of a Bayesian approach [4–12] for the solution of an inverse problem involving the estimation of some thermal parameters fields in a two-dimensional heat conduction problem. The physical problem is formulated in terms of the nodal strategy advanced in [2,3], so that the inverse problem is linear. Both the minimisation of the *Maximum a Posteriori Objective Function* (MAP) and *Monte Carlo Markov Chain* (MCMC) methods, such as the *Metropolis–Hastings* (MH) algorithm are examined as applied to the inverse problem under picture, as described below. The algorithms are tested with direct simulations obtained with a finite volume model for two kinds of samples: periodic square media and a crack in a homogeneous medium. The effects of both measurement and model errors on the estimation results are also analysed.

2. Physical problem and mathematical formulation

The physical problem examined in this article involves two-dimensional transient heat conduction in a plate, with spatially varying thermal conductivity and volumetric heat capacity. Boundaries are supposed insulated. This situation can be found when testing a thin layer medium with partial lumping across the plate. For thick samples, the possible separation of in-plane and out-of-plane temperature distribution has been discussed in [3]. Both internal steady heat generation and convective heat losses are also considered. The initial temperature within the medium is non-uniform due to the initial randomly distributed photo-thermal heat pulse. The mathematical formulation for this problem is given by:

$$C(x,y)\frac{\partial T}{\partial t} = \frac{\partial}{\partial x}\left[k(x,y)\frac{\partial T}{\partial x}\right] + \frac{\partial}{\partial y}\left[k(x,y)\frac{\partial T}{\partial y}\right] - h(x,y)(T-T_\infty) + g(x,y) \tag{1a}$$

in $0 < x < L_x$, $0 < y < L_y$, for $t > 0$

$$\frac{\partial T}{\partial x} = 0 \quad \text{at } x = 0 \text{ and } x = L_x, \text{ for } t > 0 \tag{1b}$$

$$\frac{\partial T}{\partial y} = 0 \quad \text{at } y = 0 \text{ and } y = L_y, \text{ for } t > 0 \tag{1c}$$

$$T(x,y,0) = T_0(x,y) \quad \text{for } t = 0, \text{ in } 0 < x < L_x,\ 0 < y < L_y \tag{1d}$$

where $C(x,y)$ is the local volumetric heat capacity in $\mathrm{J\,m^{-3}\,K^{-1}}$, $k(x,y)$ is the local thermal conductivity in $\mathrm{W\,m^{-1}\,K^{-1}}$, $h(x,y)$ is the local convective heat transfer coefficient in $\mathrm{W\,m^{-2}\,K^{-1}}$ and $g(x,y)$ is the local heat source, in $\mathrm{W\,m^{-3}}$.

In the *direct problem* associated with the mathematical formulation of such physical problem, the thickness of the medium and the spatial variations of the volumetric heat capacity, thermal conductivity and initial temperature are known. The objective of the direct problem is then to determine the transient temperature variation within the medium.

3. Nodal strategy and predictive model for the solution of the inverse problem

In this article we deal with the solution of an *inverse problem* involving the identification of inclusions or non-homogeneities in a heterogeneous medium. This is accomplished through the identification of the spatially-dependent thermal parameters, by making use of the nodal strategy advanced in [2,3].

For the solution of the inverse problem, we assume that transient temperature measurements are available at several positions within the medium. The temperature measurements are assumed to be taken with an infrared camera. Such measurement technique is quite powerful because it can provide accurate non-intrusive measurements, with fine spatial resolutions and at large frequencies.

For the application of the nodal strategy [2,3] we rewrite Eq. (1a) in the following non-conservative form:

$$\frac{\partial T}{\partial t} = a(x,y)\nabla^2 T + \frac{1}{C(x,y)}\left[\frac{\partial k(x,y)}{\partial x}\frac{\partial T}{\partial x} + \frac{\partial k(x,y)}{\partial y}\frac{\partial T}{\partial y}\right] - H(x,y)(T-T_\infty) + G(x,y) \tag{2}$$

where

$$a(x,y) = \frac{k(x,y)}{C(x,y)}, \quad H(x,y) = \frac{h(x,y)}{C(x,y)} \quad \text{and} \quad G(x,y) = \frac{g(x,y)}{C(x,y)}$$

An explicit discretisation of Eq. (2) using finite-differences results in:

$$Y_{i,j}^{n+1} = L_{i,j}^{n} a_{i,j} + Dx_{i,j}^{n}\delta_{i,j}^{x} + Dy_{i,j}^{n}\delta_{i,j}^{y} - \Delta t\big(T_{i,j}^{n} - T_{\infty}\big)H_{i,j} + \Delta t G_{i,j} \tag{3}$$

where the subscripts pair (i, j) denotes the finite-difference node at $x_i = i\Delta x$, $i = 1, \ldots, n_i$, and $y_j = j\Delta y$, $j = 1, \ldots, n_j$, and the superscript n denotes the time $t_n = n\Delta t$, $n = 0, \ldots, (n_t - 1)$. The other quantities appearing in Eq. (3) are given by:

$$Y_{i,j}^{n+1} = T_{i,j}^{n+1} - T_{i,j}^{n} \tag{4a}$$

$$L_{i,j}^{n} = \Delta t\left(\frac{T_{i-1,j}^{n} - 2T_{i,j}^{n} + T_{i+1,j}^{n}}{(\Delta x)^2} + \frac{T_{i,j-1}^{n} - 2T_{i,j}^{n} + T_{i,j+1}^{n}}{(\Delta y)^2}\right) \tag{4b}$$

$$Dx_{i,j}^{n} = \frac{\Delta t}{2\Delta x}\big(T_{i+1,j}^{n} - T_{i-1,j}^{n}\big) \tag{4c}$$

$$Dy_{i,j}^{n} = \frac{\Delta t}{2\Delta y}\big(T_{i,j+1}^{n} - T_{i,j-1}^{n}\big) \tag{4d}$$

$$\delta_{i,j}^{x} = \frac{1}{C(x,y)}\frac{\partial k}{\partial x} \tag{4e}$$

and

$$\delta_{i,j}^{y} = \frac{1}{C(x,y)}\frac{\partial k}{\partial y} \tag{4f}$$

Eq. (4a) defines the forward temperature difference in time. Eq. (4b) approximates the Laplacian of temperature at time t_n and node (i, j). Eqs. (4c,d), are relative to the spatial derivatives of temperature.

By writing Eq. (3) for a given node (i, j) and all time-steps, we obtain:

$$\mathbf{Y_{ij}} = \mathbf{J_{ij}}\mathbf{P_{ij}} \tag{5}$$

where

$$\mathbf{J_{ij}} = \begin{bmatrix} L_{i,j}^{1} & Dx_{i,j}^{1} & Dy_{i,j}^{1} & -\Delta t(T_{i,j}^{1} - T_{\infty}) & \Delta t \\ L_{i,j}^{2} & Dx_{i,j}^{2} & Dy_{i,j}^{2} & -\Delta t(T_{i,j}^{2} - T_{\infty}) & \Delta t \\ \vdots & \vdots & \vdots & \vdots & \vdots \\ L_{i,j}^{n_t} & Dx_{i,j}^{n_t} & Dy_{i,j}^{n_t} & -\Delta t(T_{i,j}^{n_t} - T_{\infty}) & \Delta t \end{bmatrix} \tag{6a}$$

and

$$\mathbf{Y_{ij}} = \begin{bmatrix} Y_{i,j}^{1} \\ Y_{i,j}^{2} \\ \vdots \\ Y_{i,j}^{n_t} \end{bmatrix} \tag{6b}$$

$$\mathbf{P_{ij}} = \begin{bmatrix} a_{i,j} \\ \delta_{i,j}^{x} \\ \delta_{i,j}^{y} \\ H_{i,j} \\ G_{i,j} \end{bmatrix} \tag{6c}$$

The vector of parameters at node (i, j) such as defined by Eq. (6c) contains the following parameters:

$a_{i,j}$, which is the local thermal diffusivity in $\mathrm{m^2\,s^{-1}}$.
$\delta_{i,j}^{x}$ and $\delta_{i,j}^{y}$, which are the local thermal conductivity gradients along the x and y directions, respectively, divided by the heat capacity.
$H_{i,j}$ is the local heat transfer convective coefficient divided by the local heat capacity, similar to a velocity in $\mathrm{m\,s^{-1}}$.
$G_{i,j}$ is the local heat source divided by the local heat capacity, similar to a heating rate in $\mathrm{K\,s^{-1}}$.

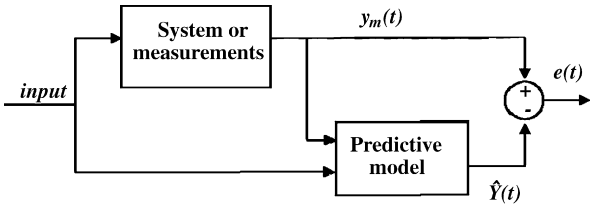

Fig. 1. Minimisation of the predictive error model.

The vector of parameters at node (i, j) contains five parameters involving only four independent functions k, C, h and g. Moreover, all the five parameters appear in Eq. (6c) are divided by C. This fact makes the simultaneous estimation of the five parameters quite ill-conditioned. However, for materials with sharp interfaces as in the cases examined herein, the thermal conductivity gradients are zero except at the interfaces. Moreover, as it will be shown by the sensitivity analysis in Section 4.2, the sensitivity coefficient with respect to the convective heat transfer coefficient is very low for the cases of interest for this work, so that this parameter can be neglected in the formulation of the problem. Also, by considering the thermal diffusivity $a = k/C$ as an unknown parameter to be estimated, instead of the thermal conductivity k, turns out that the two remaining parameters a and G are independent.

The sensitivity matrix defined in Eq. (6a) is a function of the temperature field, thus depends on these parameters. This fact would yield a non-linear estimation procedure when minimising an output error model, that is based on the difference between the direct model given by Eq. (5) and the corresponding experimental data.

One way to circumvent this problem is to use a predictive error model, such as shown in Fig. 1. In that scheme, the measurement data are directly passed to the model, seen as a predictor.

The objective function to minimise may be chosen as the L_2 norm of the predictive error $e(t)$, such as:

$$S_{i,j} = \mathbf{e}_{\mathbf{i,j}}^T \mathbf{e}_{\mathbf{i,j}} = (\mathbf{Y_{ij}} - \mathbf{J_{ij}P_{ij}})^T (\mathbf{Y_{ij}} - \mathbf{J_{ij}P_{ij}}) \tag{7}$$

In Eq. (7), the measurements in $\mathbf{Y_{ij}}$ are chosen as the "observable data" ($y_m(t)$ in Fig. 1), while the predictive model, obtained from the sensitivity matrix, is also built with the experimental data ($\hat{Y}(t)$ in Fig. 1).

Eq. (5), when used as a predictor, yields a linear dependence of the system response with respect to the vector of parameters, based on the knowledge of the sensitivity matrix. With the spatial resolution and frequency of measurements made available by infrared cameras, the sensitivity matrix can be approximately computed with the measurements [2,3]. It is of interest to point out that the choice is made to solve simultaneously as many local linear estimation problems as supplied by the measurement device (for instance the number of pixels). In this paper, we utilise a Bayesian approach [4–12] for the solution of the parameter estimation problem (7). In next sections, the subscript relative to the node (i, j) is omitted in order to simplify the notation, but the estimation still is made locally at each node.

4. Bayesian approach for the solution of inverse problems

In the Bayesian approach to statistics, an attempt is made to utilise all available information in order to reduce the amount of uncertainty present in an inferential or decision-making problem. As new information is obtained, it is combined with any previous information to form the basis for statistical procedures. The formal mechanism used to combine the new information with the previously available information is known as Bayes' theorem [4,5,9–11]. Therefore, the term *Bayesian* is often used to describe the so-called *statistical inversion approach*, which is based on the following principles [4]:

1. All variables included in the model are modeled as random variables.
2. The randomness describes the degree of information concerning their realisations.
3. The degree of information concerning these values is coded in probability distributions.
4. The solution of the inverse problem is the posterior probability distribution.

Bayes' theorem can then be stated as [4,5,9–11]:

$$\pi_{\text{posterior}}(\mathbf{P}) = \pi(\mathbf{P}|\mathbf{Y}) = \frac{\pi_{\text{prior}}(\mathbf{P})\pi(\mathbf{Y}|\mathbf{P})}{\pi(\mathbf{Y})} \tag{8}$$

where $\pi_{\text{posterior}}(\mathbf{P})$ is the posterior probability density, that is, the conditional probability of the parameters $\mathbf{P}$ given the measurements $\mathbf{Y}$; $\pi_{\text{prior}}(\mathbf{P})$ is the prior density, that is, the coded information about the parameters prior to the measurements; $\pi(\mathbf{Y}|\mathbf{P})$ is the likelihood function, which expresses the likelihood of different measurement outcomes $\mathbf{Y}$ with $\mathbf{P}$ given; and $\pi(\mathbf{Y})$ is the marginal probability density of the measurements, which plays the role of a normalising constant.

If we assume the parameters and the measurement errors to be independent Gaussian random variables, with known means and covariance matrices, and that the measurement errors are additive, a closed form expression can be derived for the posterior probability density. In this case, the *likelihood function* can be expressed as [4,5,9–11]:

$$\pi(\mathbf{Y}|\mathbf{P}) = (2\pi)^{-M/2}\left|\mathbf{W}^{-1}\right|^{-1/2}\exp\left[-\frac{1}{2}(\mathbf{Y}-\mathbf{Y}_e)^T\mathbf{W}(\mathbf{Y}-\mathbf{Y}_e)\right] \tag{9}$$

where $\mathbf{Y}_e$ is the vector of estimated variables, obtained from the solution of the forward model with an estimate for the parameters $\mathbf{P}$, M is the number of measurements and $\mathbf{W}$ is the inverse of the covariance matrix of the errors in $\mathbf{Y}$.

Similarly, for the case involving a prior normal distribution for the parameters we can write:

$$\pi(\mathbf{P}) = (2\pi)^{-n_P}|\mathbf{V}|^{-1/2}\exp\left[-\frac{1}{2}(\mathbf{P}-\boldsymbol{\mu})^T\mathbf{V}^{-1}(\mathbf{P}-\boldsymbol{\mu})\right] \tag{10}$$

where $\boldsymbol{\mu}$ and $\mathbf{V}$ are the known mean and covariance matrix for $\mathbf{P}$, respectively.

By substituting Eqs. (9) and (10) into Bayes' theorem, except for the normalising constant in the denominator we obtain:

$$\ln\left[\pi(\mathbf{P}|\mathbf{Y})\right] \propto -\frac{1}{2}\left[(M+N)\ln 2\pi + \ln\left|\mathbf{W}^{-1}\right| + \ln|\mathbf{V}| + S_{\mathrm{MAP}}(\mathbf{P})\right] \tag{11}$$

where

$$S_{\mathrm{MAP}}(\mathbf{P}) = \left[\mathbf{Y}-\mathbf{T}(\mathbf{P})\right]^T\mathbf{W}\left[\mathbf{Y}-\mathbf{T}(\mathbf{P})\right] + (\boldsymbol{\mu}-\mathbf{P})^T\mathbf{V}^{-1}(\boldsymbol{\mu}-\mathbf{P}) \tag{12}$$

Eq. (11) reveals that the maximisation of the posterior distribution function can obtained with the minimisation of the objective function given by Eq. (12), denoted as the *maximum a posteriori objective function* [4,5,9–11]. Eq. (12) clearly shows the contributions of the likelihood and of the prior distributions in the objective function, given by the first and second terms on the right-hand side, respectively.

For linear estimation problems such as the one considered here, the minimisation of the maximum a posteriori objective function is obtained with [11]:

$$\hat{\mathbf{P}}_{\mathrm{MAP}} = \left[\mathbf{J}^T\mathbf{W}\mathbf{J} + \mathbf{V}^{-1}\right]^{-1}\left[\mathbf{J}^T\mathbf{W}\mathbf{Y} + \mathbf{V}^{-1}\boldsymbol{\mu}\right] \tag{13}$$

It is apparent in Eq. (13) how the prior information is used as a regularisation term. Obviously, when the prior information for the parameters is poor, the diagonal terms of the covariance matrix are very large, and the MAP estimator tends towards the maximum likelihood estimator, and there is no regularisation effect.

On the other hand, if different *prior* probability densities are assumed for the parameters, the Posterior Probability Distribution may not allow an analytical treatment. In this case, Markov Chain Monte Carlo (MCMC) methods are used to draw samples of all possible parameters, so that inference on the posterior probability becomes inference on the samples [4,5,9].

In order to implement the Markov Chain, a density $q(\mathbf{P}^*, \mathbf{P}^{(t-1)})$ is required, which gives the probability of moving from the current state in the chain $\mathbf{P}^{(t-1)}$ to a new state $\mathbf{P}^*$.

The Metropolis–Hastings algorithm [4,5,9] was used in this work to implement the MCMC method. It can be summarised in the following steps:

1. Sample a *Candidate Point* $\mathbf{P}^*$ from a jumping distribution $q(\mathbf{P}^*, \mathbf{P}^{(t-1)})$.
2. Calculate:

$$\alpha = \min\left[1, \frac{\pi(\mathbf{P}^*|\mathbf{Y})q(\mathbf{P}^{(t-1)}, \mathbf{P}^*)}{\pi(\mathbf{P}^{(t-1)}|\mathbf{Y})q(\mathbf{P}^*, \mathbf{P}^{(t-1)})}\right] \tag{14}$$

3. Generate a random value U which is uniformly distributed on $(0, 1)$.
4. If $U \leqslant \alpha$, define $\mathbf{P}^t = \mathbf{P}^*$; otherwise, define $\mathbf{P}^t = \mathbf{P}^{(t-1)}$.
5. Return to step 1 in order to generate the sequence $\{\mathbf{P}^1, \mathbf{P}^2, \ldots, \mathbf{P}^n\}$.

In this way, we get a sequence that represents the posterior distribution and inference on this distribution is obtained from inference on the samples $\{\mathbf{P}^1, \mathbf{P}^2, \ldots, \mathbf{P}^n\}$. We note that values of $\mathbf{P}^i$ must be ignored until the chain has converged to equilibrium. For more details on theoretical aspects of the Metropolis–Hastings algorithm and MCMC methods, the reader should consult Refs. [4,5,9].

In the nodal strategy described in Section 3, the sensitivity matrix is approximately computed with the measurements. Therefore, for the implementation of the Metropolis–Hastings algorithm the uncertainties in the computation of the sensitivity matrix need to be taken into account. By assuming that $\mathbf{P}$ and $\mathbf{J}$ are independent random variables, the sought *posterior probability density* is then given by [4]:

$$\pi(\mathbf{P}, \mathbf{J}|\mathbf{Y}) \propto \pi(\mathbf{Y}|\mathbf{P}, \mathbf{J})\pi(\mathbf{P})\pi(\mathbf{J}) \tag{15}$$

where $\pi(\mathbf{J})$ is the *a priori* distribution for the sensitivity matrix $\mathbf{J}$.

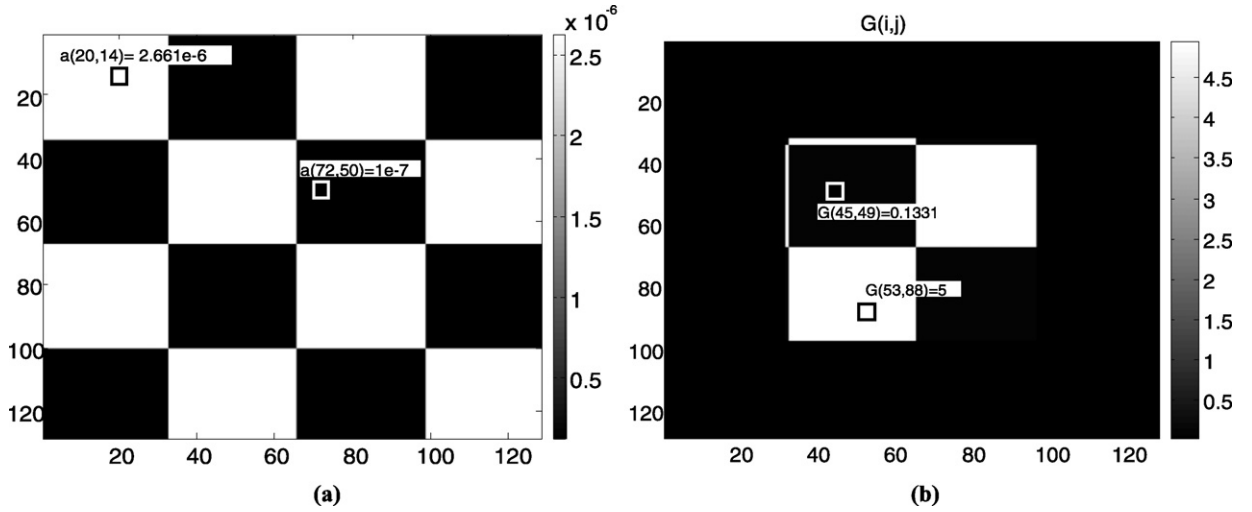

Fig. 2. (a) Distribution of materials A and B in a periodic square medium and (b) steady heat source distribution.

5. Sensitivity analysis and prior information

The cases examined below involve a thin plate, basically composed of two distinct base materials. The materials are interposed in different ways in order to examine test-cases involving different functional forms for the thermal diffusivity and heat source fields. For the sensitivity analysis and for the discussion of the prior information required for the solution of the inverse problem within the Bayesian framework, we consider in this section a periodic square arrangement of the base materials.

The following thermal properties are considered here for such materials:

$$k_A = 10\,\mathrm{W\,m^{-1}\,K^{-1}}, \quad C_A = 3.75\times10^{6}\,\mathrm{J\,m^{-3}\,K^{-1}}, \quad a_A = 2.66\times10^{-6}\,\mathrm{m^2\,s^{-1}}$$
$$k_B = 0.01\,\mathrm{W\,m^{-1}\,K^{-1}}, \quad C_B = 1\times10^{5}\,\mathrm{J\,m^{-3}\,K^{-1}}, \quad a_B = 1.0\times10^{-7}\,\mathrm{m^2\,s^{-1}}$$

Both the thermal diffusivity and heat source distributions are shown in Figs. 2(a) and (b). The scales on the axes correspond to the pixel number. The thermal properties of the materials A and B are chosen in order to be representative of a medium with a wide range of thermal diffusivity. A steady heat source term is considered applied within the medium, with strength $g = 5\times10^{5}\ \mathrm{W\,m^{-3}}$ and with the spatial distribution shown in Fig. 2(b). Hence the non-zero values to be retrieved are $G_A = 5\ \mathrm{K\,s^{-1}}$ and $G_B = 0.133\ \mathrm{K\,s^{-1}}$ respectively, as shown by the index value in Fig. 2(b).

In order to avoid the inverse crime of using the same direct solution for the generation of the simulated measurements and for the solution of the inverse problem, a finite-volume solution algorithm was developed that yields the simulated data. For the solution of the inverse problem, the plate is discretized with $n_i = n_j = 128$ internal nodes where the values of the parameters in $\mathbf{P_{ij}}$ were estimated. The space step is chosen according to the pixel size: $\Delta x = 200$ μm. In this case, the width and length of the plate are 0.0256 m.

The plate is initially randomly excited with a pseudorandom binary sequence (PRBS), hence the initial temperature field is randomly distributed as 20 or 40 °C [2]. This distribution is chosen in order to enhance the thermal gradients within the plate, and consequently the local sensitivity coefficients. The heat transfer coefficient is assumed to have a constant value equal to 10 $\mathrm{W\,m^{-2}\,K^{-1}}$. The temperature fields for $t = 0$ s and $t = 2$ s, are presented in Figs. 3(a) and (b).

For heterogeneous media involving sharp interfaces between homogeneous materials, such as shown in Fig. 2, the parameters $\delta^x_{i,j}$ and $\delta^y_{i,j}$ are zero except at the interfaces. For such cases, it was noticed in [2] that not considering these parameters in the inverse analysis do not affect the estimation of the local thermal diffusivity within the homogeneous parts of the medium, but only yields a bias at the interfaces. Therefore, these parameters are not included in the following analysis in the parameter vectors to be retrieved. Obviously, this would not be the case for materials with smooth variations of the thermophysical properties, such as functionally graded materials (FGM) or randomly variable physical properties in dispersed systems [13].

5.1. Sensitivity analysis

A sensitivity analysis is now made in order to examine the effects of the heat losses on the surface of the plate, as well as the possibility of estimating the aimed thermal diffusivity and heat source mapping. The reduced sensitivity coefficients with respect to H_{ij}, G_{ij} and a_{ij} are plotted in Figs. 4(a) and (b) as a function of time for a specific pixel. The reduced sensitivity coefficients are calculated by multiplying the original sensitivity coefficients, obtained from each element of the

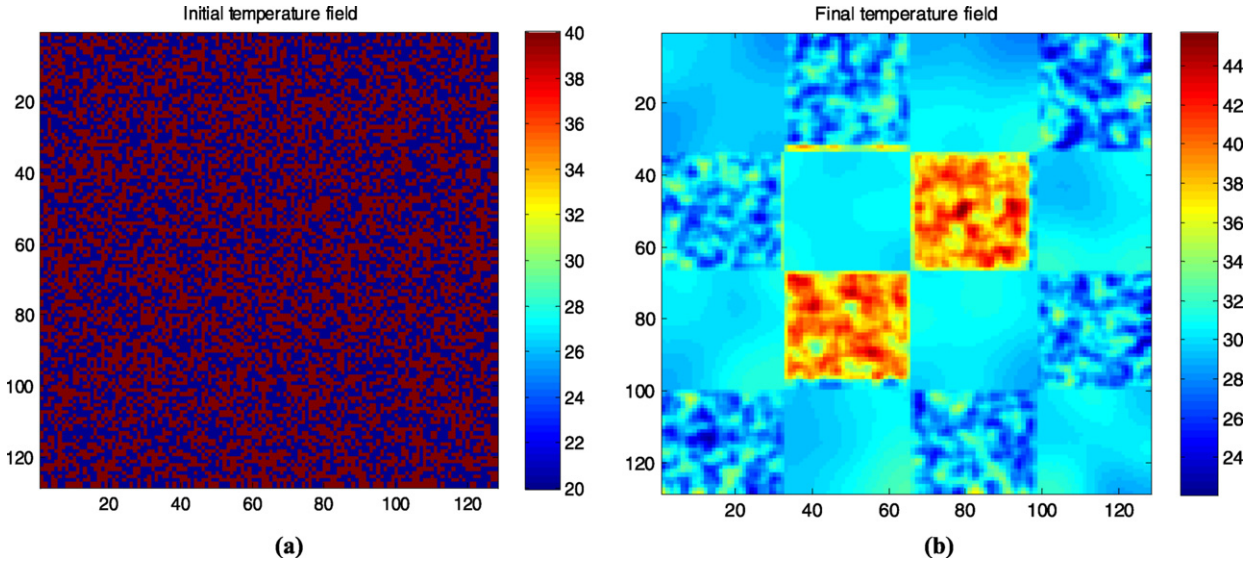

Fig. 3. (a) Initial and (b) final temperature field ($t = 2$ s).

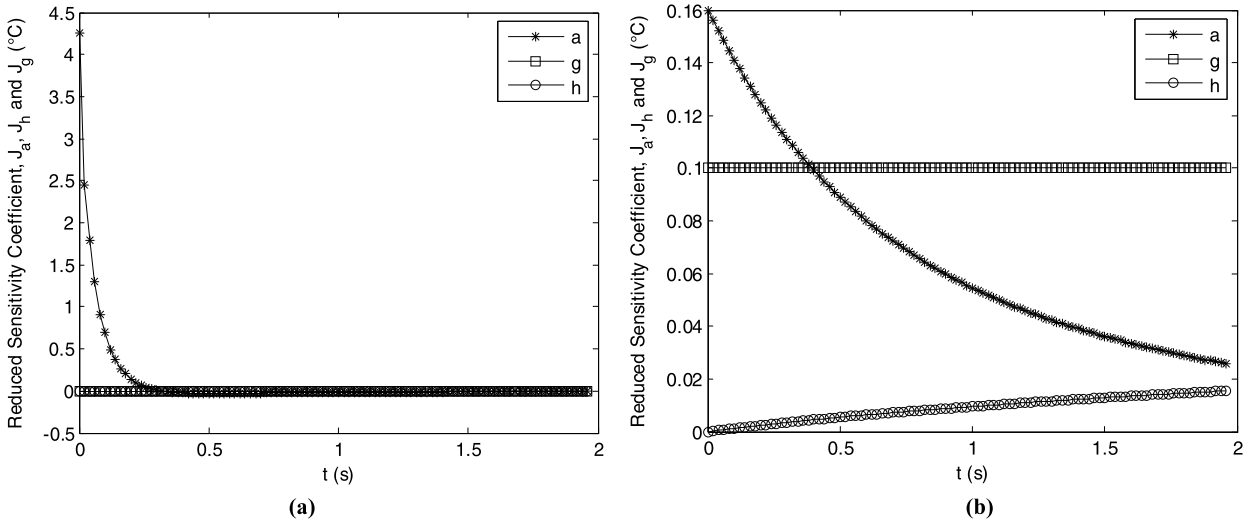

Fig. 4. Reduced sensitivity coefficients for two pixels (a) material A and (b) material B.

sensitivity matrix given by Eq. (6), by the parameters that they correspond to. Fig. 4(a) presents the reduced sensitivity coefficients at a pixel corresponding to material A, while Fig. 4(b) corresponds to a pixel in the material B. It must also be pointed out that Fig. 4(a) is relative to a pixel where the heat source is zero, while Fig. 4(b) is for a pixel where the heat source is $g = 5 \times 10^5\ \mathrm{W\,m^{-3}}$. For both pixels, the reduced sensitivity coefficient with respect to heat losses is practically zero; hence, the parameter H cannot be accurately estimated with the proposed experimental procedure, but, at the same time, it does not significantly affect the temperature field in the region. On the other hand, the reduced sensitivity coefficients with respect to thermal diffusivity attain relatively large values. The reduced sensitivity coefficient with respect to G is zero in Fig. 4(a), because the heat source is null at such specific pixel. On the other, Fig. 4(b) shows that the reduced sensitivity coefficient with respect to G is constant at locations where the heat source term is non-zero. In fact, the sensitivity coefficient with respect to G is given by Δt, as shown by the sensitivity matrix, Eq. (6). We note that the reduced sensitivity coefficients shown in Figs. 4(a) and (b) can vary from pixel to pixel not only due to the different base materials and existence of source term, but also because of the initial random flash excitation, such as shown in Fig. 3(a). However, the reduced sensitivity coefficients presented in Figs. 4(a) and (b) remain representative of those for different pixels.

Note also in Figs. 4(a) and (b) that, after passing through a maximum value at small times, the reduced sensitivity coefficients with respect to the thermal diffusivity tend to zero quite fast, especially for the most diffusive material A. Indeed, for times larger than 2 s, these reduced sensitivity coefficients become relatively small and the information provided by the temperature measurements for the estimation of such parameter is drastically reduced. Moreover, as the reduced

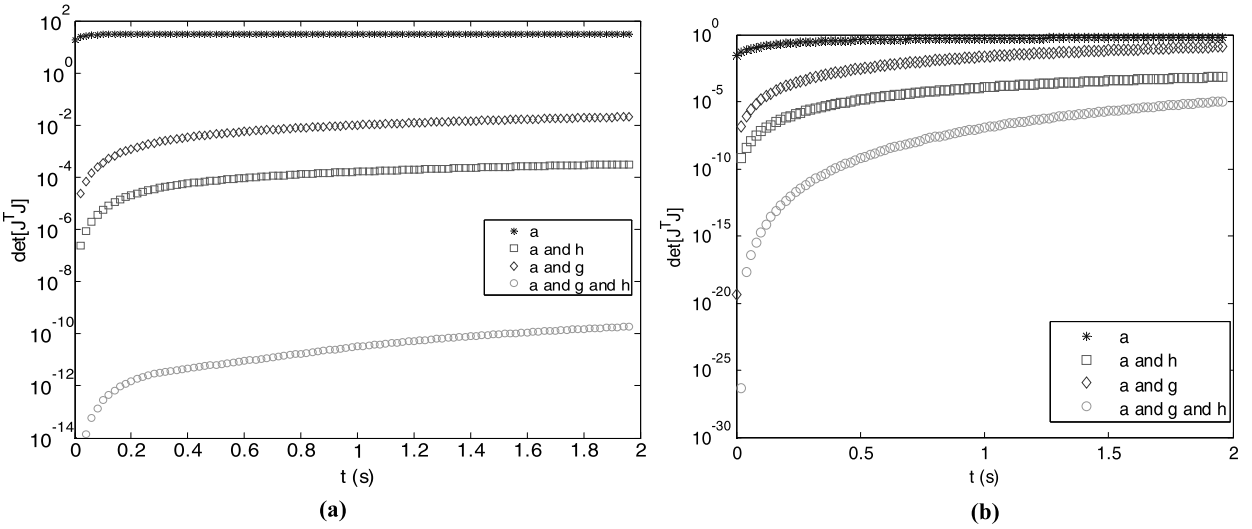

Fig. 5. Determinant of $\mathbf{J}_{\mathbf{ij}}^{T}\mathbf{J}_{\mathbf{ij}}$ for different models for two pixels (a) material A and (b) material B.

sensitivity coefficients tend to zero for H and in some locations for G, the problem is highly ill-conditioned, despite the fact that at some pixels the sensitivity coefficients are linearly independent (see Fig. 4(b)). This is also apparent from the analysis of the determinant of the information matrix $\mathbf{J}_{\mathbf{ij}}^{T}\mathbf{J}_{\mathbf{ij}}$ presented in Figs. 5(a) and (b), for the same pixels examined in Figs. 4(a) and (b), respectively. In Figs. 5(a) and (b) the determinant of the information matrix are plotted for various sets of parameters to be estimated. Such figures confirms the results of the sensitivity analysis, that is, the estimation of the heat transfer coefficient must be better discarded, and that the estimation of the thermal diffusivity as a single parameter would be better conditioned ing than the simultaneous estimation of both thermal diffusivity and heat source.

These results motivated the choice of the final experimental time as $t = 1$ s. Unfortunately, this quite small final time imposes restrictions on the number of measurements available for the estimation procedure. For a measurement frequency of 50 Hz (time step $\Delta t = 0.02$ s), the number of experimental data available at each pixel is equal to 50 points.

5.2. Prior information

For the results presented below we assume that the errors in the measured temperatures are additive, uncorrelated, normally distributed, with zero mean and known constant standard deviation σ. Note that the measurements $\mathbf{Y}$ used in the linear model (5) are actually composed of the nodal temperature differences at subsequent times (see Eq. (4a)). Hence, the likelihood function $\pi(\mathbf{Y}|\mathbf{P},\mathbf{J})$ is given by Eq. (13) with covariance matrix $\mathbf{W}^{-1} = 2\sigma^2\mathbf{I}$. With such hypothesis regarding the temperature measurements, the prior distribution for the elements of the sensitivity matrix is also normal, with mean values given Eq. (6a) and standard deviations deduced from Eq. (3) and the prior information, with:

$$\sigma_L = \sigma\,\Delta t\sqrt{\frac{6}{(\Delta x)^2}+\frac{6}{(\Delta y)^2}} \quad \text{for } L_{i,j}^{n} \tag{16}$$

Two different levels of temperature measurement errors are in consideration: $\sigma = 0.03\,^{\circ}\mathrm{C}$ and $\sigma = 0.2\,^{\circ}\mathrm{C}$, which correspond respectively to 0.15% and 1% of the maximum temperature difference in the medium.

For MAP estimation, the prior information for the elements of the vector of parameters $\mathbf{P}_{\mathbf{ij}}$ is taken in the form of normal distributions. The mean values for the thermal diffusivities a_{ij}, is taken as a_{A}, that is the value of thermal diffusivity of material A. The standard deviation for a_{ij} is first chosen as $4a_{\mathrm{A}}$. The mean value for the heat source term is taken as 2, while the standard deviation is chosen as $10G_{\mathrm{B}}$.

For the Markov Chain Monte Carlo (MCMC) method, the prior distributions for the thermal diffusivity field $a(x, y)$ are assumed to be uniform within the interval $[5\times10^{-9}, 9\times10^{-6}]\ \mathrm{m^2\,s^{-1}}$. Note that such interval encompasses most poor conductors and does not provide any practical restriction to the values to be estimated for the parameters. The prior distributions for the heat source parameters are assumed to be uniform within the interval $[0, 10]\ \mathrm{K\,s^{-1}}$.

6. Results

The Markov chain for each pixel consisted of 1600 states, where the first 800 were neglected for the computation of the statistics for the parameters. Generally, the acceptance ratio in the MH algorithm was of the order of 40% for measurements with standard deviation errors of 0.03 °C and 60% for measurements with standard deviation errors of 0.2 °C an example of

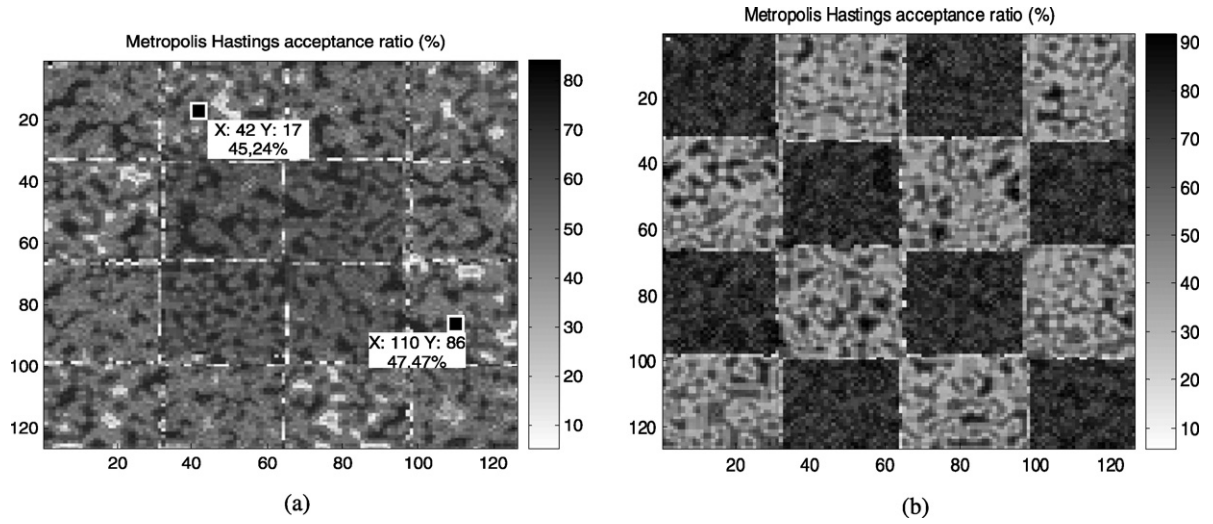

Fig. 6. MH acceptance ratio (a) $\sigma = 0.03\,^{\circ}\mathrm{C}$ and (b) $\sigma = 0.2\,^{\circ}\mathrm{C}$.

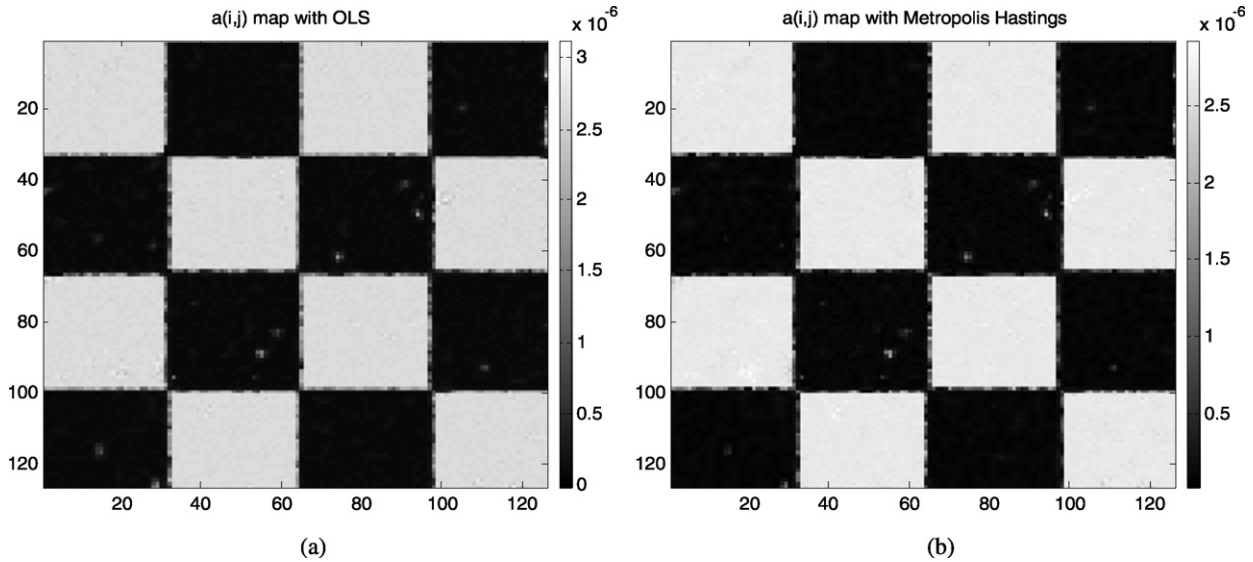

Fig. 7. $a(i, j)$ mapping for $\sigma = 0.03\,^{\circ}\mathrm{C}$ (a) with OLS (b) MCMC.

acceptance map is drawn in Fig. 6, for (a) $\sigma = 0.03\,^{\circ}\mathrm{C}$ and (b) $\sigma = 0.2\,^{\circ}\mathrm{C}$ respectively. The amplitude chosen for moving the parameters was about 1% for thermal diffusivity and sensitivity matrix, and 3% for the heat source term.

6.1. Periodic medium with $\sigma = 0.03\,^{\circ}\mathrm{C}$

Figs. 7(a) and (b) present a comparison of the estimated thermal diffusivity fields retrieved with ordinary-least squares (OLS), and the Markov Chain Monte Carlo (MCMC) method implemented via the Metropolis–Hastings (MH) algorithm. Figs. 8(a) and (b) present the retrieved source terms with OLS and MCMC methods. A comparison of these results with the exact fields shown in Figs. 2(a) and (b) reveals that the MCMC method is capable of reasonably recovering the heat source field, while the OLS fails if no regularisation is made. Both algorithms estimate efficiently the thermal diffusivity distribution. As expected the estimation is biased at the interfaces between the materials A and B, due to the fact that the thermal conductivity gradients have been neglected in Eq. (3), which means discarded in the corresponding terms of Eqs. (6).

Similar results are shown in Fig. 9, which presents the thermal diffusivity variations along a particular line (the line $i = 55$), obtained from OLS, MAP and MCMC and compared with the reference values. OLS and MCMC give very similar results, but with a smoother and more detailed profile for MCMC. With the value of the prior standard deviations chosen for the MAP estimator, there is no regularisation effect and the MAP results are identical to the OLS results. Some different

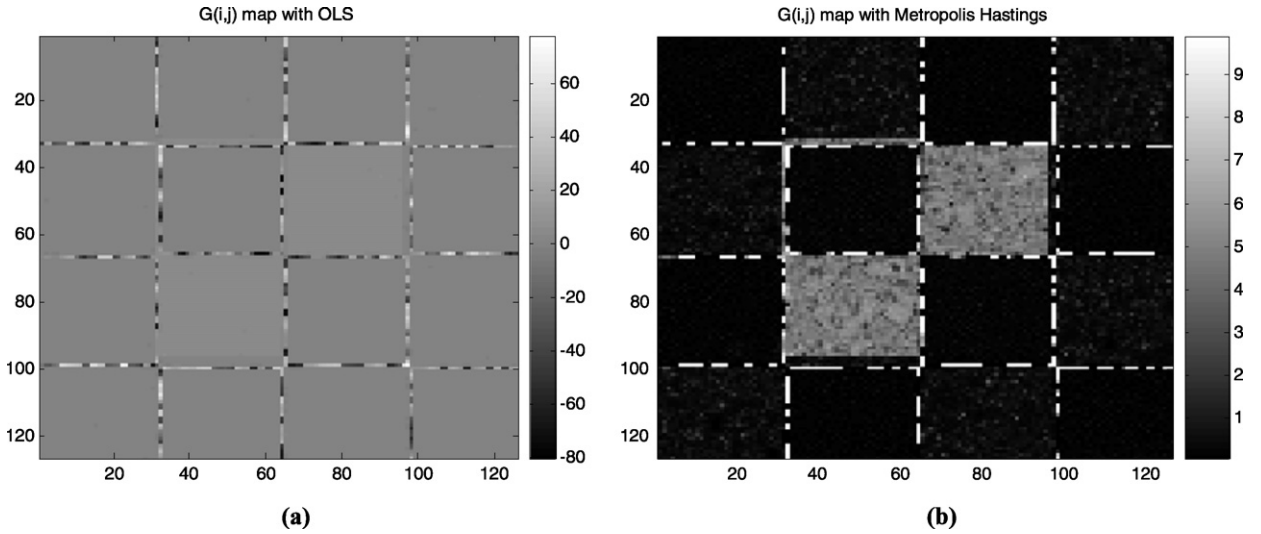

Fig. 8. $G(i, j)$ mapping for $\sigma = 0.03\,^{\circ}\mathrm{C}$ (a) with OLS (b) MCMC.

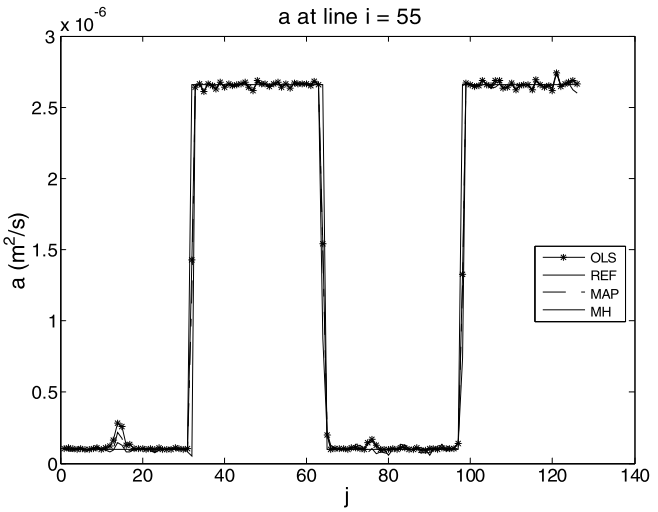

Fig. 9. Comparison of the estimated profiles of $a(i, j)$ for the line $i = 55$.

choices for the prior have been tested but are not included here for the sake of clarity. However, the main trends of the MAP estimator already deduced from Eq. (13) can be confirmed by the analysis of the results plotted in Fig. 9. Since the prior information is used as a regularisation term, a small standard deviation (corresponding to a good prior knowledge of the parameters) yields a retrieved parameter very close to the chosen prior mean values. When the STD is large there is no regularisation effect. Moreover, assuming that both the mean and STD of a Gaussian variable are known would not be far from an "inverse crime" since that would mean that the parameter distribution is already known.

Figs. 10 and 11 illustrate the resulting marginal posterior distribution and convergence behaviour of Markov chain, respectively. Fig. 10 presents the marginal posterior distributions obtained from MCMC samples for the thermal diffusivity and heat source estimated at pixel $i = 84$, $j = 49$. It can be noticed that the obtained posterior distributions closely follow a Gaussian distribution, as expected from the Gaussian likelihood and the uniform prior assumed in this work. Fig. 11 presents the evolution of the states of the chain for 1600 states at the pixel $i = 84$, $j = 49$. It can be seen from Fig. 11 that after the burning states, the chain reached the convergence rapidly.

The standard deviation of the marginal posterior distributions can be averaged over the estimated fields in order to evaluate the global dispersion of the retrieved parameters. These values are compared with the corresponding standard deviations obtained with OLS. The results are given in Table 1. Previous comments about the performance of the MCMC method are confirmed in this table, since the average standard deviations remain lower for this algorithm than for OLS.

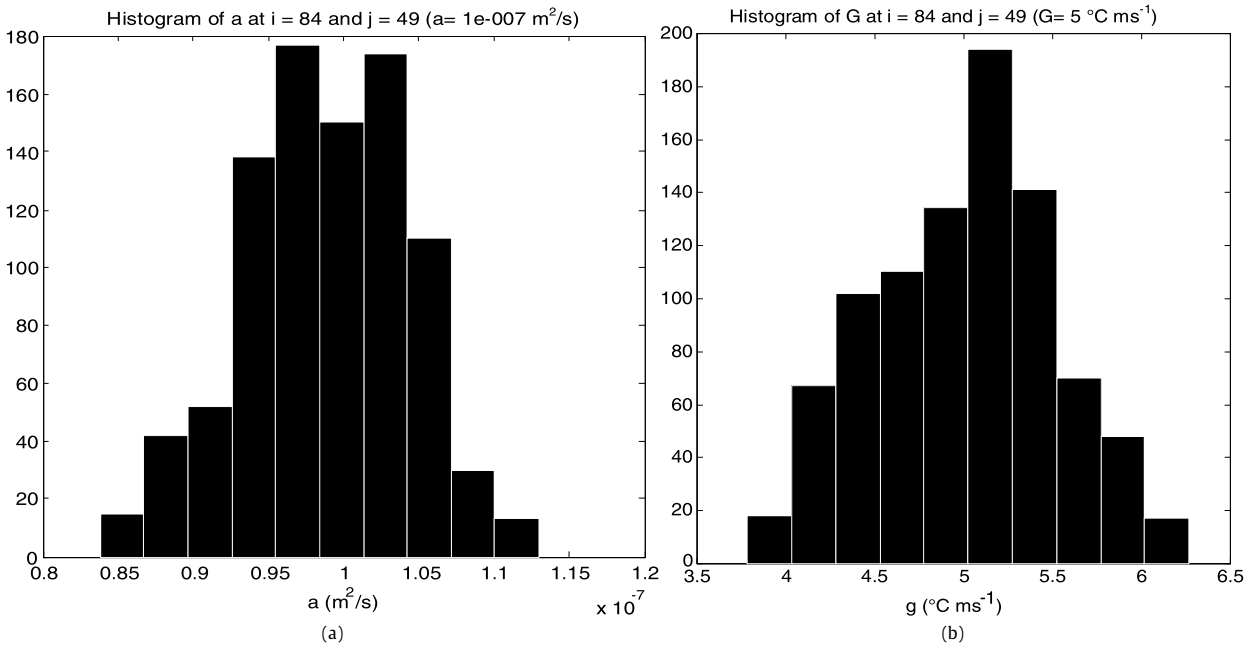

Fig. 10. Posterior distributions at pixel (84, 49) (a) $a(i, j)$ and (b) $G(i, j)$.

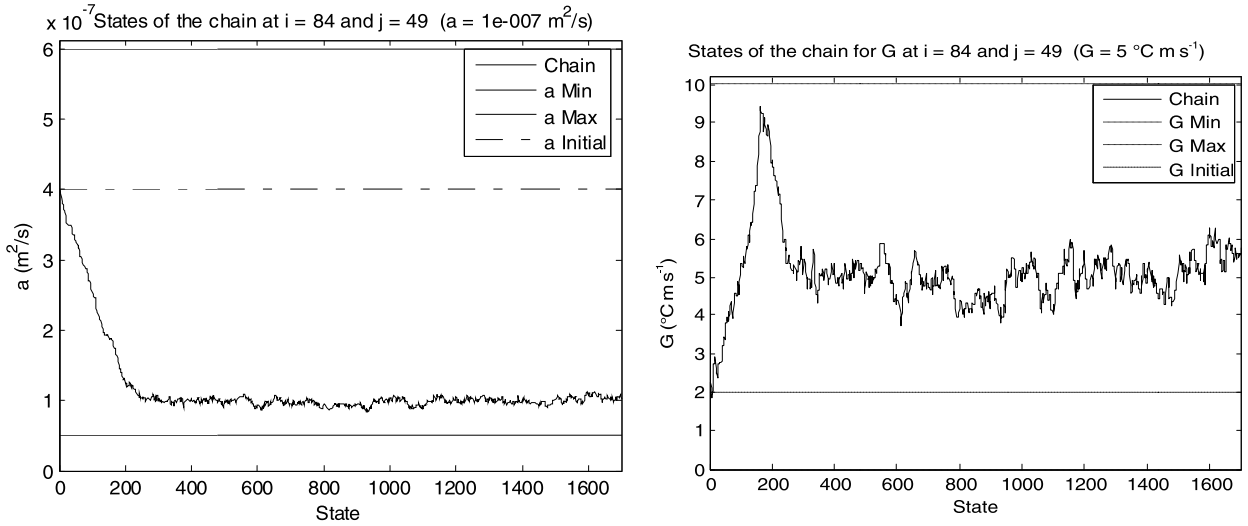

Fig. 11. Evolution of Markov chains.

Table 1
Average standard deviation for OLS and MCMC methods.

Case	Method	Thermal diffusivity ($m^2\,s^{-1}$) $\sigma = 0.03\,°C$	Heat source ($K\,s^{-1}$) $\sigma = 0.03\,°C$	Thermal diffusivity ($m^2\,s^{-1}$) $\sigma = 0.2\,°C$	Heat source ($K\,s^{-1}$) $\sigma = 0.2\,°C$
Periodic	OLS	2.9×10^{-8}	0.64	1.4×10^{-7}	2.7
Periodic	MH	1.6×10^{-8}	0.24	7.2×10^{-8}	0.75
Crack	OLS	1.4×10^{-8}	0.32	–	–
Crack	MH	9.9×10^{-9}	0.23	–	–

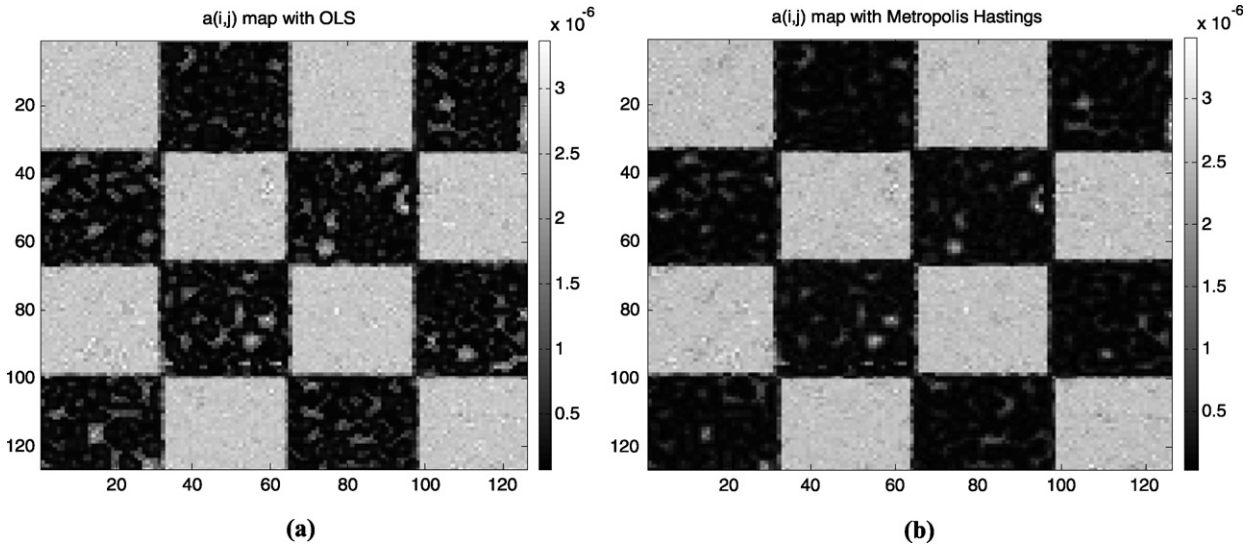

Fig. 12. $a(i, j)$ map for $\sigma = 0.2\,^{\circ}\mathrm{C}$ (a) with OLS, (b) MCMC.

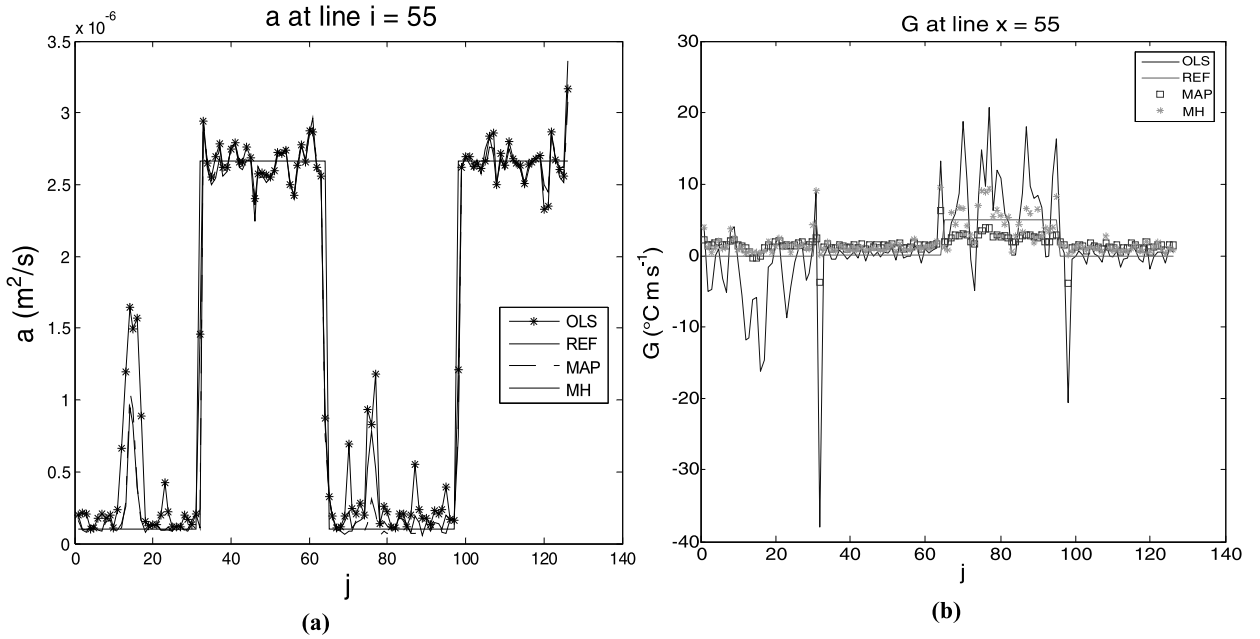

Fig. 13. Profiles for the line $i = 55$ (a) $a(i, j)$ and (b) $G(i, j)$.

6.2. Periodic medium with $\sigma = 0.2\,^{\circ}\mathrm{C}$

The same estimation approaches examined above are now compared for errors in the measured temperatures of standard deviation $\sigma = 0.2\,^{\circ}\mathrm{C}$. The estimated thermal diffusivity fields are shown in Figs. 12(a) and (b). It is apparent in these images that the MCMC method yields smoother results than the OLS approach.

Both the retrieved thermal diffusivity and heat source profiles along the line $i = 55$ are also plotted in Figs. 13(a) and (b). For this high level of noise, the MCMC method still yields better results than OLS for the heat source map. However, the heat source distribution is quite poorly retrieved by both the OLS and MCMC method, as shown in Figs. 14(a) and (b), when compared with the reference map given in Fig. 2(b).

The average standard deviations of the marginal posterior distributions given by the MCMC approach are lower than the corresponding standard deviations obtained with OLS, as shown in Table 1. In fact, the results shown in this table seem to indicate that the difference of performances between the OLS and MCMC methods grows with the level of noise in the data.

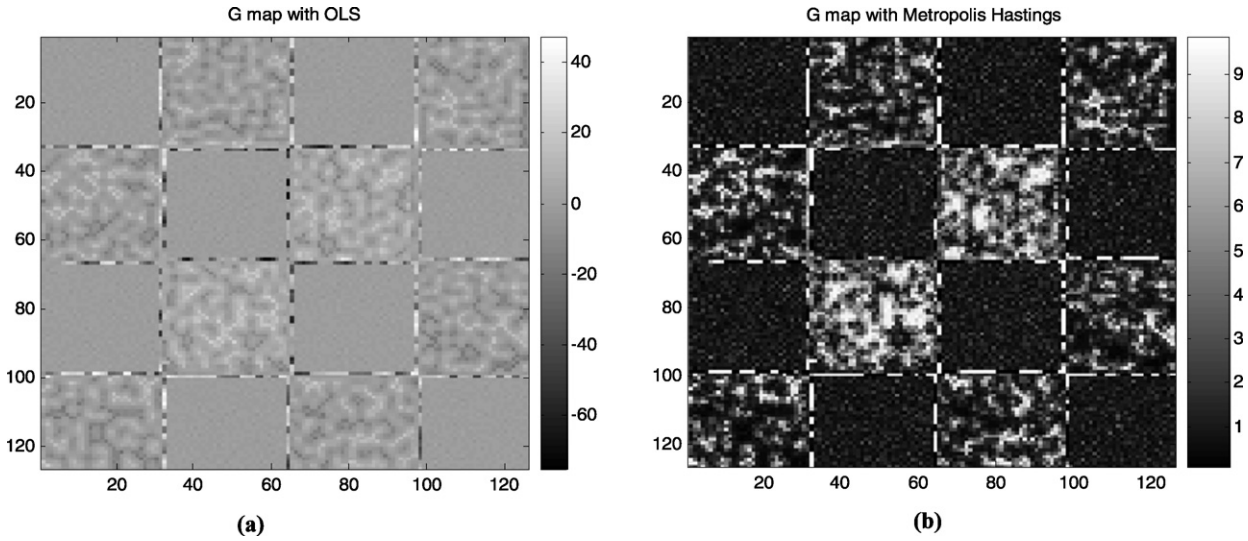

Fig. 14. G map for $\sigma = 0.2\,^{\circ}\mathrm{C}$ (a) OLS and (b) MCMC.

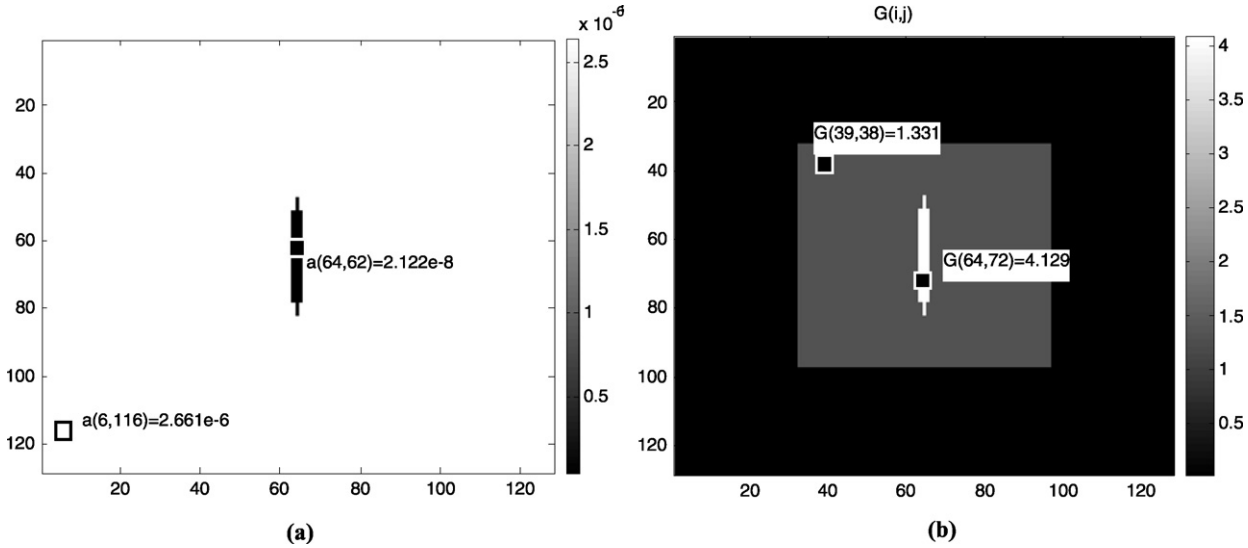

Fig. 15. Crack medium (a) $a(i, j)$ and (b) $G(i, j)$.

6.3. Crack in a homogeneous medium

The medium is composed with a homogeneous material A and an insulating crack B with thermal properties such that

$$k_{\mathrm{A}} = 10\,\mathrm{W\,m^{-1}\,K^{-1}}, \quad C_{\mathrm{A}} = 3.75 \times 10^{6}\,\mathrm{J\,m^{-3}\,K^{-1}}, \quad a_{\mathrm{A}} = 2.66 \times 10^{-6}\,\mathrm{m^{2}\,s^{-1}}$$
$$k_{\mathrm{B}} = 0.0257\,\mathrm{W\,m^{-1}\,K^{-1}}, \quad C_{\mathrm{B}} = 1\,211\,025\,\mathrm{J\,m^{-3}\,K^{-1}}, \quad a_{\mathrm{B}} = 2.12 \times 10^{-8}\,\mathrm{m^{2}\,s^{-1}}$$

The crack has approximately a rectangular shape and is located in the center of the material. It has $2\Delta x$ by $26\Delta x$, as illustrated in Figs. 15(a) and (b), for the thermal diffusivity and heat source distributions, respectively. The scales on the axes correspond to the pixel number. The applied steady heat source term is $g = 5 \times 10^{6}\ \mathrm{W\,m^{-3}}$. Hence the non-zero values to be retrieved are $G_{\mathrm{A}} = 1.33\ \mathrm{K\,s^{-1}}$ and $G_{\mathrm{B}} = 4.129\ \mathrm{K\,s^{-1}}$ respectively, as shown by the index value in Fig. 15(b). In Figs. 16(a) and (b) are shown both the initial and final temperature fields.

The standard deviation of the temperature measurements is $\sigma = 0.03\,^{\circ}\mathrm{C}$. The amplitude chosen for moving the parameters was 1% for thermal diffusivity, 2% for moving the sensitivity matrix, and 13% for the heat source term. The Markov chain for each pixel consisted of 1500 states, where the first 500 were neglected for the computation of the statistics for the parameters. Generally, the acceptance ratio in the MH algorithm was of the order of 10%.

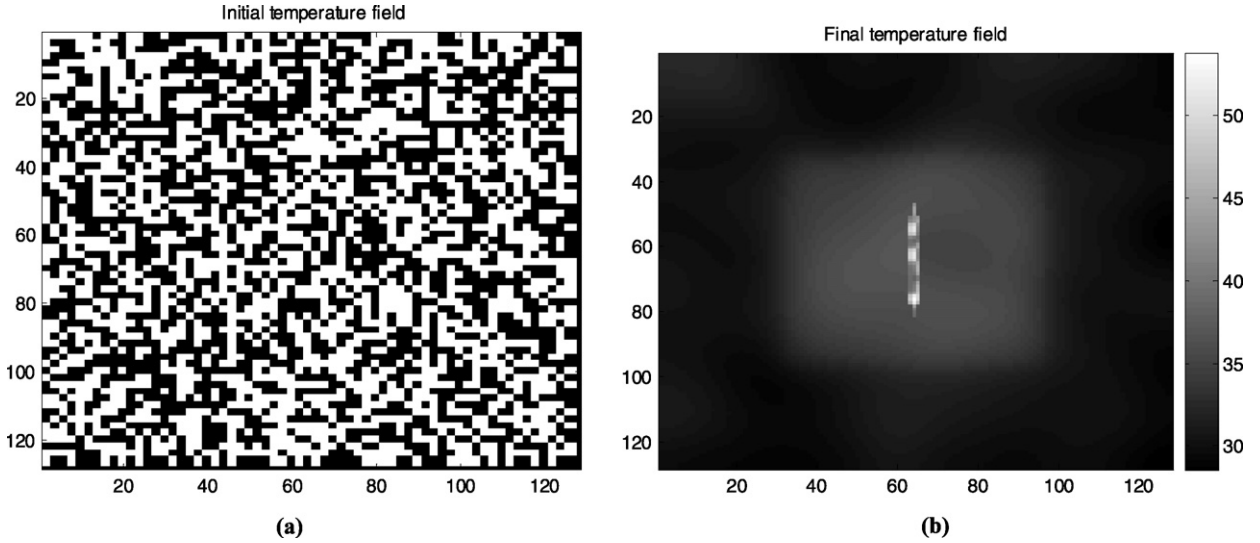

Fig. 16. (a) Initial and (b) final temperature field.

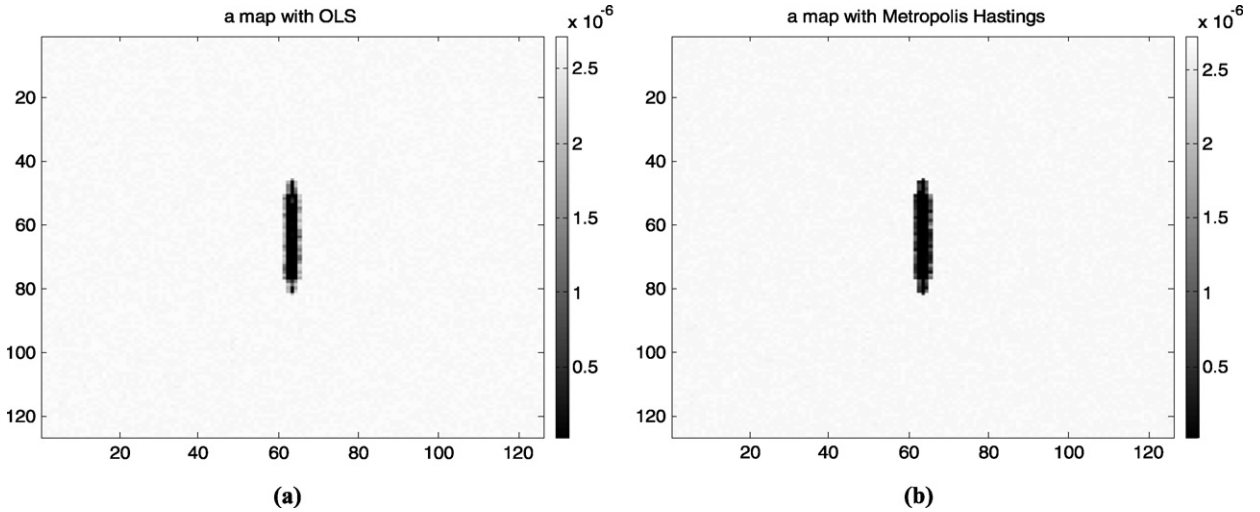

Fig. 17. Thermal diffusivity mapping with a crack (a) OLS and (b) MCMC.

Figs. 17(a) and (b) show a comparison of the estimated thermal diffusivity fields retrieved by the OLS and MCMC methods, while the retrieved heat source maps, obtained with such methods, are presented in Figs. 18(a) and (b). Both algorithms estimate reasonably the thermal diffusivity distribution. The OLS fails to retrieve the heat source map if no regularisation is made. The MCMC method is capable of reasonably recovering the heat source field. These results are confirmed by the analysis of the standard deviation maps, as shown in Figs. 19(a) and (b), as well as the average values given in Table 1.

Since simulated data are used herein, it is easy to compute the root mean square error (RMS). The RMS error is defined here as

$$e_{\mathrm{RMS}} = \sqrt{\frac{1}{I.J}\sum_{j=1}^{J}\sum_{i=1}^{I}\left[a_{\mathrm{est}}(i,j) - a_{\mathrm{ex}}(i,j)\right]^2} \tag{17}$$

where

e_{RMS} is the RMS error;
a_{est} is the estimated thermal diffusivity at position i, j;
a_{ex} is the exact thermal diffusivity at position i, j;
I, J is the size of the matrix of measurements.

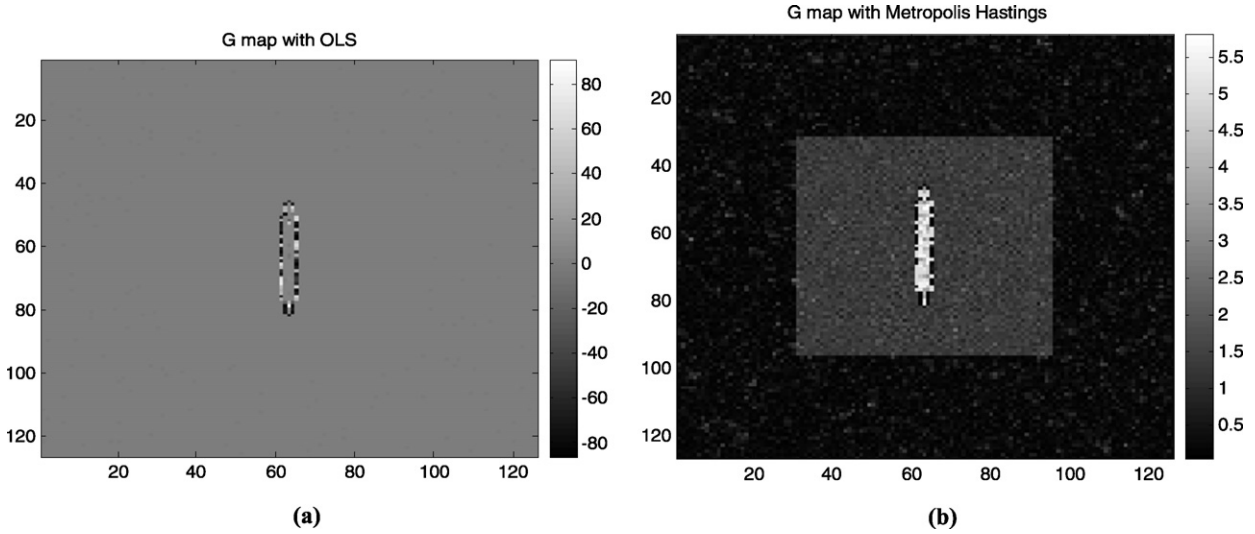

Fig. 18. Heat source mapping with a crack (a) OLS and (b) MCMC.

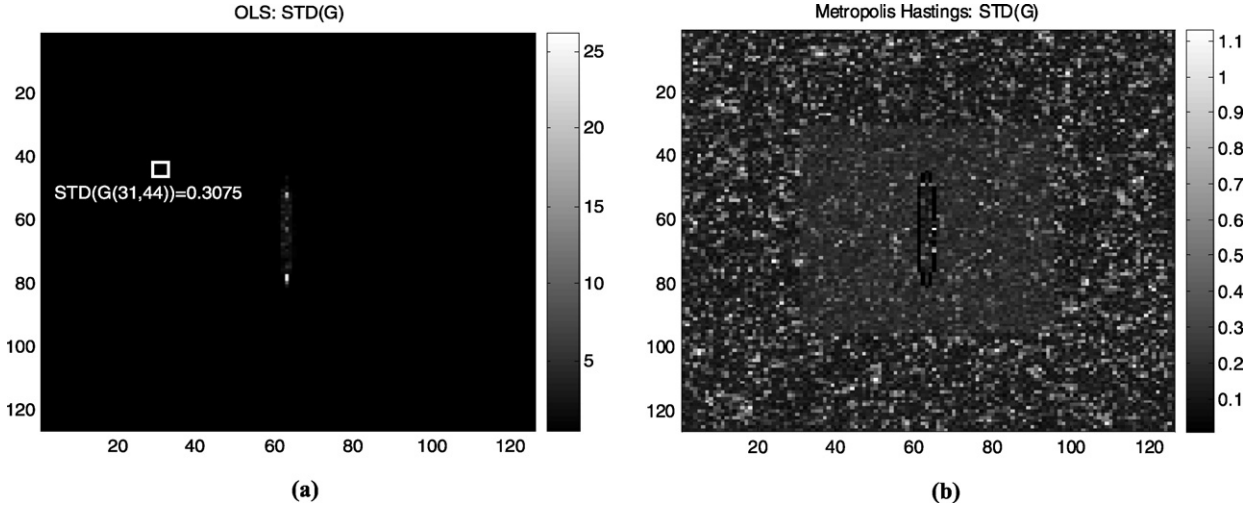

Fig. 19. Posterior average standard deviation mapping (a) OLS and (b) MCMC.

Table 2
RMS error (crack case).

Method	Thermal diffusivity RMS error ($m^2\,s^{-1}$)	Heat source RMS error ($K\,s^{-1}$)
OLS	6.8×10^{-8}	4.2
MCMC	1.3×10^{-7}	0.4

Table 2 presents the RMS errors for the results obtained with both the OLS and MCMC methods for the crack case. As for the cases examined above involving the periodic medium, Table 2 shows that the heat source term can only be accurately estimated with the MCMC method.

The computational times for the estimation of the thermal diffusivities with OLS were of the order of 1 s. Due to the sampling procedure, the MH algorithm required 360 s for the results shown in the figures hereafter. These computational times were obtained with a code developed under the MATLAB Platform, run in a Pentium 2.4 GHz, with 3 GB of RAM memory.

7. Conclusions

In this article the solution of a 2D inverse problem dealing with the identification of non-homogeneities or inclusions in a medium with steady heat sources was proposed, through the simultaneous estimation of spatially-dependent thermophysical properties and heat source. A two-dimensional heat conduction problem was used for the comparison of different techniques for the solution of the inverse problem. The heat conduction equation was written in a non-conservative form, as a predictive model, in order to apply a nodal strategy that results in a linear estimation problem. In such form of the heat conduction equation, the spatially dependent thermal diffusivity and heat source appear explicitly. For the experimental conditions examined in this paper, involving a material composed of homogeneous base materials with sharp interfaces between them, and natural convective heat losses at the surface of the plate, the thermal conductivity gradient and heat transfer coefficient were neglected in the inverse analysis.

The linear inverse problem resulting from the nodal approach was solved with an Ordinary Least Squares estimator, and within a Bayesian frame with the Maximum A Priori estimator, and the approach of the Markov Chain Monte Carlo method based on the Metropolis–Hastings algorithm. Among the techniques examined, only the Markov Chain Monte Carlo was capable of accurately predicting both the spatially varying thermal diffusivity and heat source field.

The results presented herewith with simulated temperature measurements reveal that these techniques can accurately identify non-homogeneous materials through the mapping of thermal diffusivity, even for strict cases involving sharp interfaces. Moreover, the MH algorithm seems to be relatively less sensitive to an increase in the measurement errors.

The results also showed the main problem arising with the MAP approach when a higher regularisation term is used, yielding an important bias in the estimates towards the prior information.

Future works include the implementation of this approach for the simultaneous estimation of transient thermal diffusivity and heat source fields.

Acknowledgements

This work was prepared within the scope of a CNPq (Brazil)–CNRS (France) cooperation project. The authors would also like to acknowledge partial financial support provided by CAPES and FAPERJ, agencies from the Brazilian and Rio de Janeiro state government, respectively.

References

[1] L. Ljung, System Identification: Theory for the User, Prentice Hall, 1987.
[2] J.C. Batsale, J.L. Battaglia, O. Fudym, Autoregressive algorithms and spatially random flash excitation for 3D non destructive evaluation with infrared cameras, QIRT J. 1 (2004) 5–20.
[3] M. Bamford, J.C. Batsale, O. Fudym, Nodal and modal strategies for longitudinal thermal diffusivity profile estimation. Application to the non destructive evaluation of SiC/SiC composites under uniaxial tensile tests, Infrared Phys. Technol. 52 (2009) 1–13.
[4] J. Kaipio, E. Somersalo, Statistical and Computational Inverse Problems, Appl. Math. Sci., vol. 160, Springer-Verlag, 2004.
[5] S. Tan, C. Fox, G. Nicholls, Inverse Problems, Course Notes Phys., vol. 707, University of Auckland, 2006.
[6] N. Zabaras, Inverse problems in heat transfer, in: W.J. Minkowycz, E.M. Sparrow, J.Y. Murthy (Eds.), The Handbook of Numerical Heat Transfer, 2nd ed., John Wiley & Sons, 2004, chap. 17.
[7] J. Wang, N. Zabaras, A Bayesian inference approach to the stochastic inverse heat conduction problem, Int. J. Heat Mass Transfer 47 (2004) 3927–3941.
[8] J. Wang, N. Zabaras, Using Bayesian statistics in the estimation of heat source in radiation, Int. J. Heat Mass Transfer 48 (2005) 15–29.
[9] P.M. Lee, Bayesian Statistics, Oxford Univ. Press, London, 2004.
[10] R. Winkler, An Introduction to Bayesian Inference and Decision, Probabilistic Publishing, Gainsville, 2003.
[11] J.V. Beck, K.J. Arnold, Parameter Estimation in Engineering and Science, Wiley–Interscience, New York, 1977.
[12] H.R.B. Orlande, V. Kolehmainen, J.P. Kaipio, Reconstruction of thermal conductivity and heat capacity using a tomographic approach, Int. J. Heat Mass Transfer 50 (2007) 5150–5160.
[13] C.P. Naveira, R.M. Cotta, H.R.B. Orlande, O. Fudym, Eigenfunction expansions for transient diffusion in heterogeneous media, Int. J. Heat Mass Transfer 52 (2009) 5029–5039.